Shear-Flow Dispersion, Internal Waves and Horizontal Mixing in the Ocean[1]

W. R. YOUNG[2] AND P. B. RHINES

Department of Physical Oceanography, Clark III, Woods Hole Oceanographic Institution, Woods Hole, MA 02543

C. J. R. GARRETT

Department of Oceanography, Dalhousie University, Halifax, Nova Scotia, Canada

(Manuscript received 4 December 1981, in final form 19 February 1982)

ABSTRACT

Two models of advection-diffusion in the oscillatory, sheared-velocity field of an internal wave are discussed. Our goal is to develop intuition about the role of such currents in horizontal ocean mixing through the mechanism of shear dispersion. The analysis suggests simple parameterizations of this process, i.e., those in Eqs. (7), (36) and (42). The enhanced horizontal diffusion due to the interaction of the vertical diffusion and vertical shear of the wave field can be described by an "effective horizontal diffusivity" which is equal to the actual horizontal diffusivity plus a term equal to the mean-square vertical shear of horizontal displacement times the vertical diffusivity, provided the vertical length scale of the horizontal velocity field is not too small. In the limit of small vertical length scale the expression reduces to Taylor's (1953) result in which the effective horizontal diffusivity is inversely proportional to the actual vertical diffusivity.

The solutions also incidentally illuminate a variety of other advection-diffusion problems, such as unsteady shear dispersion in a pipe and enhanced diffusion through wavenumber cascade induced by steady shearing and straining velocity fields.

These solutions also serve as models of horizontal stirring by mesoscale eddies. Simple estimates of mesoscale shears and strains, together with estimates of the horizontal diffusivity due to shear dispersion by the internal wave field, suggest that horizontal mesoscale stirring begins to dominate internal-wave-shear dispersion at horizontal scales larger than 100 m.

1. Introduction

The aim of this paper is to examine some simple advection-diffusion models with the goal of developing intuition about the role of sheared oscillatory currents in horizontally mixing tracers in the ocean interior. The velocity fields considered are so simple that the advection-diffusion equation can be solved exactly; we hope that our principal conclusions apply to the more complicated velocity fields associated with internal waves and inertial oscillations.

It may be that the horizontal mixing of tracers produced by the combined action of internal-wave vertical shear and vertical mixing is significant in both deep-ocean and shelf regions and may provide an effective mechanism for horizontally dispersing tracer anomalies on length scales which are so small that the vigorous mesoscale stirring is unimportant. Another goal of this presentation is to estimate the length scale at which this mesoscale stirring begins to dominate internal-wave-shear dispersion. The solutions of the advection-diffusion models discussed here suggest simple parameterizations of these processes.

Besides the real-space phenomenon of shear dispersion our solutions also illustrate an important related process in Fourier space, *viz.*, the cascade to higher wavenumbers and the consequent enhanced dissipation produced by the shearing (and straining) of tracers by a large-scale velocity field. This process is important even on basin scales; it is the mechanism by which peak concentrations are reduced. The ultimate problem is to predict the statistics of tracers in oceans with turbulence, waves and mean circulation all included. In addition to the goal of understanding the interaction of turbulence and mean flow in shaping tracer distributions, one wants to know the sampling variability to be expected with turbulence of known intensity.

The theory of shear-flow dispersion began with Taylor's (1953) realization that the sheared velocity profile in a pipe or channel would interact with cross-channel diffusion to produce an augmented along-channel dispersion. In this way a vertical sheet of dye is deformed by the shear and mixed vertically, producing a spreading plug of dye, almost uniformly

[1] WHOI Contribution No. 5093.

[2] Present affiliation: Marine Physical Laboratory, Scripps Institution of Oceanography, La Jolla CA 92093.

0022-3670/82/060515-13$07.25

distributed across the channel, which moves downstream at the cross-channel averaged velocity. The length of the plug increases as the square root of time so that the interaction of the vertical diffusion and vertical shear can be parameterized as an "effective horizontal diffusivity". Remarkably, this diffusivity is inversely proportional to the actual molecular diffusivity and is several orders of magnitude larger. Since Taylor's work the subsequent developments have relied heavily on the simplifying approximations he introduced to obtain an analytic solution. These approximations amount to assuming that the tracer is almost uniformly distributed across the channel; thus Taylor's theory applies only after the initial distribution of tracer has had sufficient time to spread across the channel.

The moment method of Aris (1956) and Saffman (1962) is not subject to the same limitations as Taylor's approximate theory and in principle it can provide precise information about the time evolution of certain integral moments (such as center of mass and moment of inertia) of tracer distributions. However, in previous geophysical applications, the limitations of Taylor's simpler theory have not been particularly restrictive because attention has been confined to shallow systems such as estuaries and streams (e.g., Fischer *et al.*, 1979). An exception is Csanady's (1966) study of shear dispersion in an Ekman layer; because the region is semi-infinite, Taylor's theory does not apply and the moment method is used.

In this article we shall discuss some models of shear dispersion in an infinite region. These models may qualitatively describe processes in the ocean interior where the shearing (and straining) of internal waves and mesoscale currents can amplify smaller scale diffusive processes. The first model we discuss is so simple that the advection-diffusion equation can be solved exactly. This observation was first made by Townsend (1951) and was first exploited in the context of shear dispersion by Okubo (1967); our analysis builds on their discussion.

This tractability arises from two idealizations:

1) The region is infinite so it is not necessary to satisfy no-flux boundary conditions.

2) The horizontal velocity field is a *linear* function of the vertical coordinate.

In discussing horizontal shear dispersion by internal waves the second idealization is potentially misleading: it is observed that the horizontal velocity fields of inertial oscillations have a jagged vertical structure with many sign reversals. Accordingly it is necessary to supplement the exact solution with an approximate analysis of shear dispersion by a horizontal velocity field with an *oscillatory* vertical structure. It is found that the exact solution, based on the above idealizations, is misleading if the vertical diffusivity is sufficiently large or the vertical length scale of the horizontal velocity sufficiently small. With reasonable values of the vertical diffusivity in the ocean we can then estimate the vertical wavenumber above which internal waves do not cause significant shear dispersion.

In Section 2 we introduce the first model of advection-diffusion in an oscillatory shear flow. In this model the horizontal velocity depends linearly on the vertical coordinate. This problem is solved exactly using an advected coordinate system. The form of the solution motivates the introduction of an "effective horizontal diffusivity" which is equal to the actual horizontal diffusivity plus a term which arises from the interaction of the vertical shear and vertical diffusivity. This result is also derived heuristically using a simple geometric argument.

In Section 3 we discuss shear dispersion in an oscillatory horizontal velocity field with a sinusoidal vertical structure. If the vertical length scale of the velocity field is sufficiently large one recovers the same effective horizontal diffusivity as in Section 2. In the other limit, when the vertical length scale of the velocity field is small, one recovers Taylor's expression for the effective horizontal diffusivity of a steady shear flow.

In Section 4 we discuss shear dispersion by the internal-wave field and give some numerical estimates of the effective horizontal diffusivity based on an empirical vertical-shear spectrum. Our estimates indicate that the horizontal diffusivity is ~ 1000 times the vertical diffusivity.

In Section 5 we discuss advection-diffusion problems in which the velocity field is steady but has some simple spatial structure, such as a pure shear or strain. These models may be relevant to the mesoscale-eddy field rather than the rapidly changing internal-wave field. In any case it is important to realize that in an unbounded medium (i.e., in configurations where no-flux boundary conditions are not imposed) steady and oscillatory velocity fields may produce qualitatively different dispersion.

Finally in Section 6 the relative strengths of shear dispersion by internal waves and mesoscale eddies are compared. We conclude that the mesoscale stirring becomes important at surprisingly small horizontal length scales (~ 100 m).

2. A model equation and its solution

The model advection-diffusion equation we will solve in this section is

$$\theta_t + u\theta_x = \eta\theta_{xx} + \kappa\theta_{zz}, \tag{1}$$

$$\theta(x, z, 0) = \cos kx \cos mz. \tag{2}$$

At first this initial condition might seem strange since

θ is negative. However, this is a Fourier component from which more general initial conditions can be built. Moreover, we can of course add a constant to it so θ is positive everywhere. The velocity field is

$$u = \alpha z \cos\omega t;$$

more general fields are considered in Sections 3 and 5. In (1) and (2) x and z are horizontal and vertical coordinates, η and κ are horizontal and vertical diffusivities and θ is the tracer concentration. Previous work on this model equation in a bounded region using Taylor's method is summarized by Fischer (1976) and Fischer *et al.* (1979). Bowden (1965) first considered alternating currents in the context of tidal mixing in a shallow channel; time dependence of the shearing current is obviously a desirable feature in a model of shear dispersion by an internal wave. The steady limit, $\omega \to 0$, is an important special case and is qualitatively different from the unsteady case.

This model equation has also been discussed by Chatwin (1975) and Okubo (1967), who in principle solved it exactly. Okubo, however, limited his treatment to a discussion of the first few moments of the tracer distribution. Kullenberg (1972) extended Okubo's analysis and provided observational confirmation of the basic effect. We will also present an exact solution using a different method which has the advantages of exposing the structure of the solution more clearly and being physically motivated.

a. The case $m = 0$

For simplicity we shall first solve (1) and (2) with $m = 0$ so that θ is initially independent of z; the case $m \neq 0$ is more complicated algebraically and is treated at the end of this section. First note that the solution of (1) and (2) if $\eta = \kappa = 0$ is

$$\theta = \cos k\tilde{x}, \tag{3}$$

where

$$\tilde{x} = x - (\alpha/\omega) z \sin\omega t. \tag{4}$$

The variable $\tilde{x}$ is an advected coordinate; it is the initial position of the particle which is at x at time t. The solution (3) is simply a statement that when there is no diffusion each particle retains its initial value of θ.

Now suppose η and κ are nonzero. The exact solution can be found by looking for a solution of the form

$$\theta = A(t) \cos k\tilde{x}, \tag{5}$$

where $A(0) = 1$. When (5) is substituted into (1) one finds

$$\frac{dA}{dt} = -[\eta k^2 + \kappa k^2(\alpha/\omega)^2 \sin^2\omega t]A.$$

The solution of this simple differential equation is

$$\theta = \exp\left\{-\eta k^2 t - \tfrac{1}{2}\kappa k^2(\alpha/\omega)^2 \times \left[t - \frac{\sin 2\omega t}{2\omega}\right]\right\} \cos k\tilde{x}. \tag{6}$$

A is plotted as a function of time in Fig. 1. When (α/ω) is sufficiently small $A(t)$ is essentially a decaying exponential with small "bumps" due to the $\sin 2\omega t$ in (6).

The solution (6) shows that the interaction between the shear flow with the vertical diffusion produces an "effective" horizontal diffusivity

$$\eta_e = \eta + \tfrac{1}{2}(\alpha/\omega)^2\kappa \tag{7}$$

(the limit $\omega \to 0$ is singular and is discussed in the Section 5).[3] Eq. (7) is one of the most important results in this study; it is implicit in the expression for the increase of the second moment given by Okubo (1967) and has been noted and applied by Garrett and Loder (1981).

b. A different initial condition

In order to illustrate the role of the effective horizontal diffusivity more clearly we use Fourier analysis to solve (1) with a more interesting initial condition

$$\theta(x, z, 0) = \frac{\sqrt{\pi}}{2a} \exp(-x^2/4a^2) = \int_0^\infty \exp(-a^2k^2) \cos kx\, dk. \tag{8}$$

Since (6) is the solution of (1) with $\cos kx$ as an initial condition, from (8) the solution with a Gaussian initial condition is

$$\theta(x, z, t) = \int_0^\infty \exp(-a^2k^2) \exp[-\eta_e k^2 t + \tfrac{1}{2}\kappa(\alpha/\omega)^2 k^2(\sin 2\omega t/2\omega)] \cos k\tilde{x}\, dk = \frac{\sqrt{\pi}}{2\tilde{a}} \exp(-\tilde{x}^2/4\tilde{a}^2),$$

where $\tilde{x}$ is defined in (4), η_e in (7) and

$$\tilde{a}^2 = a^2 + \eta_e t - \tfrac{1}{2}\kappa(\alpha/\omega)^2(\sin 2\omega t/2\omega). \tag{9}$$

[3] Dr. R. Smith (1982a) has observed that if the velocity field in (1) is altered by replacing ωt by $\omega t + \phi$ then $\eta_e - \eta$ in (7) is increased by the phase dependent factor $(1 + 2\sin^2\phi)$. With $\phi \neq 0$, however, the particles do not oscillate symmetrically about their initial positions and the increase in the diffusivity can be thought of as vertical diffusion due to the mean z-structure of the tracer distribution. This process is physically distinct from shear dispersion and in any case is absent from the more realistic problem discussed in Section 3.

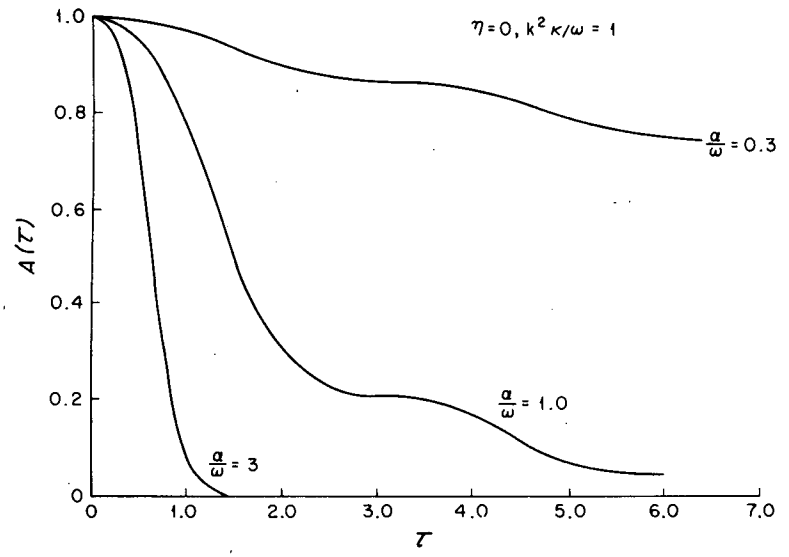

FIG. 1. The amplitude A in (5) as a function of the nondimensional time $\tau = \alpha t$. For simplicity $\eta = 0$ so that the decay is due solely to the interaction of the shear with the vertical diffusivity.

Eq. (9) shows clearly how the width-squared of the Gaussian distribution of tracer increases linearly with time in a manner consistent with the interpretation of η_e as an effective horizontal diffusivity. Note that even if the actual horizontal diffusivity η is identically zero the combination of a shear current and vertical diffusion produces horizontal spreading.

c. *A geometric derivation of (7)*

There is a simple physical argument which also gives result (7) and so provides some useful insight into the process of shear dispersion in an oscillatory flow.

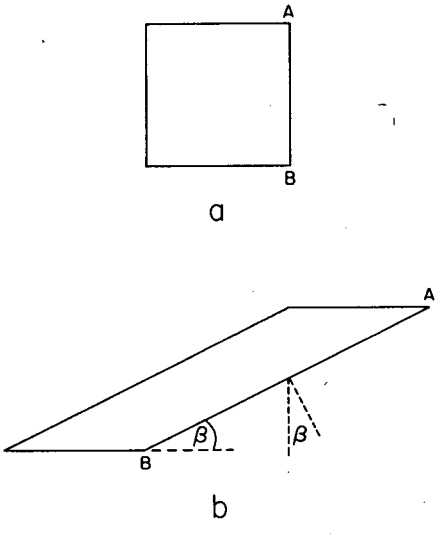

FIG. 2. (a) The initial configuration of a fluid element. The θ-isopleths are vertical. (b) At some later time the square is distorted by the shear flow into a trapezoid. The θ-isopleths make an angle β with the horizontal.

Consider a fluid element that initially has a square cross section in the x-z plane (see Fig. 2). The shear flow subsequently deforms it into a trapezoid. We shall calculate the vertical flux of θ through the face bounded by AB.

First observe that

$$[\text{vertical flux through AB}] = -\kappa \frac{\partial \theta}{\partial z} = -\kappa \frac{\partial \theta}{\partial x} \cot\beta, \quad (10)$$

where β is the angle the tilted θ-isopleths make with the horizontal.

Second the line segment AB is extended so that there is a greater area for the vertical flux of θ:

$$[\text{length of AB}] = [\text{initial length of AB}] \csc\beta. \quad (11)$$

Third,

$$[\text{projection of vertical } \theta\text{-gradient onto the normal to AB}] = \cos\beta. \quad (12)$$

To calculate the integrated vertical flux through AB we multiply (10), (11) and (12) together to obtain

$$[\text{integrated flux through AB}] = -\kappa \frac{\partial \theta}{\partial x} \cot^2\beta. \quad (13)$$

Finally, noting that

$$\cot\beta = \frac{\alpha}{\omega} z \sin\omega t$$

and time-averaging (13) over a period,

[average integrated flux through AB]

$$= -\frac{1}{2}\left(\frac{\alpha}{\omega}\right)^2 \kappa \frac{\partial \theta}{\partial x}.$$

Adding this to the flux due to the actual horizontal diffusivity, $-\eta \partial\theta/\partial x$, shows that the combination in (7) appears naturally as an effective horizontal diffusivity.

d. The case $m \neq 0$

We now turn to the solution of (1) and (2) when $m \neq 0$. The algebra here is a bit involved but the principal conclusion is easily summarized: the horizontal dispersion of the tracer field is consistent with the interpretation of η_e in (7) as an effective horizontal diffusivity provided

$$\kappa m k \alpha/\omega^2 \ll 1.$$

Since this condition can be rewritten as

$$\frac{m}{k} \ll \left(\frac{\omega}{\alpha}\right)\left(\frac{\omega}{\kappa k^2}\right), \tag{14}$$

and low diffusivity and high frequencies are the most interesting cases, Eq. (14) is not a very restrictive condition on the aspect ratio of the initial condition.

e. Details of the solution with $m \neq 0$

It is easy to see that the solution of (1) and (2) has the form

$$\theta = a(t) \cos k\tilde{x} \cos mz + b(t) \sin k\tilde{x} \sin mz, \tag{15}$$

$$a(0) = 1 \quad \text{and} \quad b(0) = 0, \tag{16}$$

where $\tilde{x}$ is defined in (4). When (15) is substituted into (1), the resulting evolution equations for a and b are

$$\frac{da}{dt} = -[\kappa(m^2 + k^2\tilde{x}_z^2) + \eta k^2]a + 2\kappa m k \tilde{x}_z b, \tag{17}$$

$$\frac{db}{dt} = -[\kappa(m^2 + k^2\tilde{x}_z^2) + \eta k^2]b + 2\kappa m k \tilde{x}_z a. \tag{18}$$

The above are simplified to

$$\frac{d\hat{a}}{dt} = 2\kappa m k \tilde{x}_z b, \tag{19}$$

$$\frac{d\hat{b}}{dt} = 2\kappa m k \tilde{x}_z a, \tag{20}$$

by introducing

$$\hat{a} = \exp\left[\int_0^t \{\kappa(m^2 + k^2\tilde{x}_z^2) + \eta k^2\} dt'\right] a, \tag{21}$$

$$\hat{b} = \exp\left[\int_0^t \{\kappa(m^2 + k^2\tilde{x}_z^2) + \eta k^2\} dt'\right] b. \tag{22}$$

Now observe that (19) and (20) have a first integral

$$\hat{a}^2 - \hat{b}^2 = \text{constant},$$
$$= 1 \text{ from (16), (21) and (22),}$$

which can be used to put (19) in the form

$$\pm \frac{d\hat{a}}{\sqrt{\hat{a}^2 - 1}} = 2\kappa m k \tilde{x}_z dt.$$

Integrating the above and using (21) and (22) we have finally

$$a = \exp[-(\eta_e k^2 t + \kappa m^2 t) + \tfrac{1}{4}\kappa k^2(\alpha^2/\omega^3) \sin 2\omega t] \cosh[2\kappa m k(\alpha/\omega^2)(\cos\omega t - 1)], \tag{23}$$

$$b = \exp[\quad \text{As Above} \quad] \sinh[\quad \text{As Above} \quad], \tag{24}$$

where η_e is defined in (7). Note how (23) and (24) reduce to (6) when $m = 0$. If (14) is satisfied then $a(t)$ in (23) is essentially a decaying exponential with an e-folding scale of $(\eta_e k^2 + \kappa m^2)^{-1}$ while $b(t)$ is small for all time. Thus, subject to the mild restriction (14), η_e in (7) is an effective horizontal diffusivity for initial conditions with $m \neq 0$.

f. Elliptically-polarized horizontal-velocity fields

To complete this section we discuss the solution of

$$\theta_t + u\theta_x + v\theta_y = \eta(\theta_{xx} + \theta_{yy}) + \kappa\theta_{zz}, \tag{25}$$

$$\theta(x, y, z, 0) = \cos kx \cos l\left(y - \frac{\beta}{\omega} z \sin\phi\right), \tag{26}$$

$$(u, v) = [\alpha z \cos\omega t, \beta z \cos(\omega t + \phi)]. \tag{27}$$

Elliptically polarized velocity fields like (27) are characteristic of internal waves. Note in the initial condition (26) that the y-structure is contrived so that the particles oscillate symmetrically about their initial positions. This device removes the mean vertical structure which gives rise to the phase-dependent effects referred to in the earlier footnote. As in

the previous example we define advected coordinates

$$\left.\begin{aligned}\tilde{x} &= x - (\alpha/\omega)z\sin\omega t\\ \tilde{y} &= y - (\beta/\omega)z\sin(\omega t + \phi)\end{aligned}\right\},$$

and look for the solution of the form

$$\theta = A(t)\cos k\tilde{x}\cos l\tilde{y}.$$

The algebra is straightforward and almost identical to that of the previous example. One finds that the horizontal spread of the tracer is characterized by a diffusivity tensor

$$\eta_e = \begin{bmatrix}\overline{\tilde{x}_z^2} & \overline{\tilde{x}_z\tilde{y}_z}\\ \overline{\tilde{x}_z\tilde{y}_z} & \overline{\tilde{y}_z^2}\end{bmatrix}\kappa + \begin{bmatrix}\eta & 0\\ 0 & \eta\end{bmatrix}$$

$$= \begin{bmatrix}\eta + \frac{1}{2}\left(\frac{\alpha}{\omega}\right)^2\kappa & \frac{1}{2}\left(\frac{\alpha\beta}{\omega^2}\right)\cos\phi\kappa\\ \frac{1}{2}\left(\frac{\alpha\beta}{\omega^2}\right)\cos\phi\kappa & \eta + \frac{1}{2}\left(\frac{\beta}{\omega}\right)^2\kappa\end{bmatrix}, \quad (28)$$

where overbar is an average over a period. Thus if $\bar{\theta}$ denotes the period-averaged tracer distribution, then

$$\bar{\theta}_t = \nabla\cdot(\eta_e\nabla\bar{\theta}),$$

where $\nabla = (\partial/\partial x, \partial/\partial y)$.

We expect inertial oscillations to make the dominant contribution to η_e in (7) and (28) because they combine the highest vertical shears α with the lowest frequencies ω. Since inertial oscillations are circularly polarized, $\phi = \pi/2$ in (27), η_e is a diagonal tensor and $\bar{\theta}$ obeys a simple isotropic diffusion equation.

3. Shear dispersion in a flow with sinusoidal vertical structure

As mentioned at the end of the last section, Eq. (7) suggests that inertial oscillations will be the most important part of the internal-wave band as far as shear dispersion is concerned, because they combine the smallest frequencies with the largest vertical shears.

The strongest objection to inserting numerical estimates of α and ω directly into (7) is the jagged vertical structure of inertial oscillations. Observations show that there is vertical structure down to scales of a meter or less.

To address this objection we will use the moment method to solve (1) with

$$u = u_0\cos mz\cos\omega t. \quad (29)$$

Before becoming involved in the algebra we will state our principal conclusion: the effective horizontal diffusivity due to the interaction of the velocity field in (29) and vertical diffusivity is

$$\eta_e = \eta + \frac{1}{4}\left(\frac{u_0^2}{\omega}\right)\left(\frac{\kappa_*}{1+\kappa_*^2}\right), \quad (30a)$$

or

$$\eta_e = \eta + \frac{1}{4}\left(\frac{m^2u_0^2}{\omega^2}\right)\left[\frac{\kappa}{1+(m/m_*)^4}\right], \quad (30b)$$

where κ_* is a nondimensional vertical diffusivity and m_* is a nondimensional wavenumber

$$\kappa_* = \kappa m^2/\omega, \quad (31a)$$

$$m_*^2 = \omega\kappa^{-1}. \quad (31b)$$

When $\kappa_* \ll 1$, Eq. (7) is recovered if we interpret α^2 as the mean-square vertical shear, $\frac{1}{2}m^2u_0^2$. On the other hand if $\kappa_* \gg 1$ we find $\eta_e - \eta$ is inversely proportional to κ, a result strongly reminiscent of Taylor's (1953) steady-pipe-flow theory. The result (30) will be discussed more thoroughly at the end of this section. Smith (1982b) has also noted the importance of the nondimensional number κ_* in the context of oscillatory shear dispersion in bounded regions such as tidal estuaries.

a. Analysis of (1) and (29) using the moment method

We will suppose that the initial condition is

$$\theta(x, z, 0) = \theta_0(x),$$

where $\theta_0(x)$ decreases to zero as $|x| \to \infty$; z-dependent initial conditions are easily treated. Indeed it is worth remarking that since the problem we are solving is linear the vertically integrated evolution of the initial condition above is the same as the vertically integrated evolution of problems whose initial conditions satisfy

$$\theta_0(x) = \int_{-\infty}^{\infty}\theta(x, z, 0)dz.$$

We will use the notation

$$\langle a\rangle = \int_{-\infty}^{\infty} a\,dx.$$

It follows from (1) that

$$\langle\theta\rangle_t = \kappa\langle\theta\rangle_{zz}, \quad (32a)$$

$$\langle x\theta\rangle_t = \kappa\langle x\theta\rangle_{zz} + u\langle\theta\rangle, \quad (32b)$$

$$\langle x^2\theta\rangle_t = \kappa\langle x^2\theta\rangle_{zz} + 2u\langle x\theta\rangle + 2\eta\langle\theta\rangle, \quad (32c)$$

and so on for the higher moments. Because the velocity field is independent of x the moment hierarchy is closed and can be solved sequentially.

The solution of (32a) is

$$\langle\theta\rangle(z, t) = \int_{-\infty}^{\infty}\theta_0(x)dx = \text{constant},$$

and substituting this into (32b) gives

$$\langle x\theta\rangle_t - \kappa\langle x\theta\rangle_{zz} = u_0\langle\theta\rangle \cos mz \cos\omega t.$$

The solution of the above is

$$\langle x\theta\rangle/\langle\theta\rangle = (u_0/\omega)(1+\kappa_*^2)^{-1}\cos mz[\kappa_*\cos\omega t + \sin\omega t] + (\text{an exponentially decaying transient}), \quad (33)$$

where κ_* is defined in (31).

Note that because of the diffusivity the velocity of the center of mass of the tracer distribution is out of phase with the velocity field in (29). This phase lag is vitally important when we come to consider the evolution of the second moment, $\langle x^2\theta\rangle$. Substituting (33) into (32c) yields

$$\langle x^2\theta\rangle_t - \kappa\langle x^2\theta\rangle_{zz} = 2\langle\theta\rangle(u_0^2/\omega)(1+\kappa_*^2)^{-1} \times \cos^2 mz \cos\omega t[\kappa_*\cos\omega t + \sin\omega t] + 2\eta\langle\theta\rangle. \quad (34)$$

Eq. (34) can easily be solved exactly by decomposing the forcing term on the right-hand side into its fundamental z and t Fourier components and using linear superposition. However, if one's sole interest is in how rapidly the dominant horizontal length scale of the distribution is expanding, it suffices to consider the zero-frequency components of the right-hand side. Thus

$$\langle x^2\theta\rangle/\langle\theta\rangle = [\tfrac{1}{2}(u_0^2/\omega)\kappa_*(1+\kappa_*^2)^{-1} + 2\eta]t + [\text{harmonic contributions}]. \quad (35)$$

Eq. (35) shows that the effective horizontal diffusivity is

$$\eta_e = \eta + \frac{1}{4}\left(\frac{u_0^2}{\omega}\right)\left(\frac{\kappa_*}{1+\kappa_*^2}\right). \quad (36)$$

b. *Various limiting cases of (36)*

For orientation it is instructive to consider (36) in three different regimes

$$\kappa_* \ll 1: \quad \eta_e \simeq \eta + \left(\frac{mu_0}{2\omega}\right)^2\kappa, \quad (37a)$$

$$\kappa_* = 1: \quad \eta_e \simeq \eta + \tfrac{1}{8}(u_0)\left(\frac{u_0}{\omega}\right), \quad (37b)$$

$$\kappa_* \gg 1: \quad \eta_e \simeq \eta + \left(\frac{u_0}{2m}\right)^2\kappa^{-1}. \quad (37c)$$

Eq. (37a) is the result obtained in Section 2 if α^2 is identified as the mean-square shear, $\frac{1}{2}m^2u_0^2$. In this limit the θ value of a particle is approximately constant over a period and horizontal dispersion is due to the mechanism discussed physically in Section 2.

We picked $\kappa_* = 1$ in (37b) because $\kappa_*(1+\kappa_*^2)^{-1}$ achieves a global maximum here. In this case the effective horizontal diffusivity is proportional to the product of a particle excursion distance, $u_0\omega^{-1}$ and a particle velocity u_0. Thus simple mixing-length theories may give misleading results since their qualitative and quantitative validity requires that the diffusivity be neither too great nor too small.

Eq. (37c) is essentially Taylor's expression for the dispersion coefficient in steady pipe flow (note $\eta_e - \eta$ is inversely proportional to κ). The physical explanation of this surprising result is well known: in this limit the vertical diffusivity is so strong that a particle loses its value of θ *almost* as soon as it is horizontally displaced. The enhanced horizontal dispersion is due, however, to the small excursion that is possible before θ changes. The smaller the vertical diffusivity, the greater this excursion and the larger the horizontal dispersion. The pipe-flow analogy is discussed further below.

c. *Some remarks on shear dispersion in pipes*

The reduction of (36) to Taylor's pipe-flow formula when $\kappa_* \gg 1$ is not a coincidence. If θ is independent of z initially then the velocity field (29) is such that $\theta_z(x, z, t) = 0$ at $z = 0$ and π/m. Thus the problem discussed in this section can also be interpreted as shear dispersion in pipe. The walls of the pipe are at $z = 0$ and π/m where (29) automatically ensures that the no-flux boundary conditions are satisfied.

This interpretation is additional motivation for considering shear dispersion in the velocity field (29). Previous studies of unsteady shear flows (Fischer *et al.*, 1979) in pipes have used the velocity field of Section 2. Since the no-flux boundary conditions are not automatically satisfied the algebra is much more complicated and the final expression for η_e must be evaluated numerically. By contrast (36) is transparent and the limits $\kappa_* \to 0$ or ∞ are easily extracted. This last point is important since there is some confusion in the literature about the limit $\kappa_* \to 0$. Fischer *et al.* (1979) simply state that the dispersion coefficient is zero in this limit. The actual answer is given by (7) or equivalently (37a) and explained physically in Section 2. To apply the physical argument in situations where either the velocity field or the initial tracer distribution has nontrivial vertical structure one assumes that as fluid particles are swept backward and forward their θ value is essentially unchanged over a period. This assumption becomes invalid when $\kappa_* \geq O(1)$ and not surprisingly the effective diffusivity is no longer given by (7).

d. *Shear dispersion in a random velocity field*

Using the moment method it is straightforward to extend the previous results to the case where $u(z, t)$

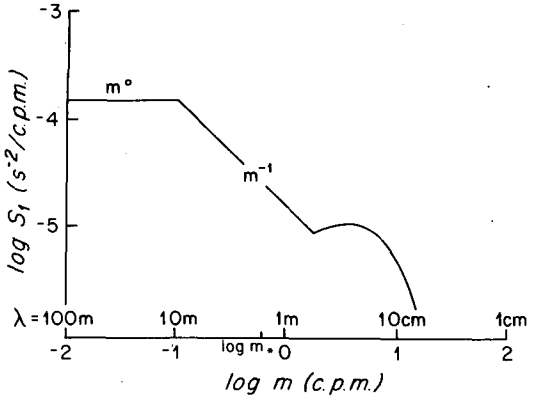

FIG. 3. A schematic illustration of the empirical shear spectrum (adapted from Gargett *et al.*, 1981). Only wavenumbers $< m_*$ contribute significantly to shear dispersion. The low (m^0) and intermediate (m^{-1}) ranges are universal to within a factor of 2 when scaled by the local buoyancy frequency (numerical values shown here are for N = 2.3 cph).

is a stationary random function of z, i.e.,

$$u(z, t) = \int_{-\infty}^{\infty} dm \int_0^{\infty} d\omega \tfrac{1}{2}[u(m, \omega)e^{i(mz-\omega t)} + (\text{complex conjugate})]. \quad (38)$$

The ensemble-average mean-square current (which can be taken as a space or time average if the waves have random phase) is

$$\bar{u}^2 = \int_{-\infty}^{\infty} dm \int_0^{\infty} d\omega \tfrac{1}{2}\overline{u(m, \omega)u^*(m, \omega)}, = \int_0^{\infty} dm \int_0^{\infty} d\omega E(m, \omega), \quad (39)$$

where the overbar is an ensemble average. The solutions of (32a, b) are $\langle\theta\rangle$ = constant and

$$\langle x\theta\rangle = \langle\theta\rangle \int_{-\infty}^{\infty} dm \int_0^{\infty} d\omega \tfrac{1}{2}(m^4\kappa^2 + \omega^2)^{-1} \times [(m^2\kappa + i\omega)u(m, \omega)e^{i(mz-\omega t)} + (\text{c.c.})]. \quad (40)$$

To obtain the evolution equation for $\overline{\langle x^2\theta\rangle}$, substitute (40) and (38) into (32c) and ensemble average. The key ingredient is

$$\overline{u\langle x\theta\rangle} = \langle\theta\rangle \int_0^{\infty} dm \int_0^{\infty} d\omega m^2\kappa \times (m^4\kappa^2 + \omega^2)^{-1}E(m, \omega) \quad (41)$$

and the final expression for η_e is

$$\eta_e = \overline{\langle x^2\theta\rangle}/2t\overline{\langle\theta\rangle}, \quad (42a)$$

$$= \eta + \int_0^{\infty} dm \int_0^{\infty} d\omega m^2\kappa \times (m^4\kappa^2 + \omega^2)^{-1}E(m, \omega). \quad (42b)$$

Assuming horizontal isotropy this may be written as

$$\eta_e = \eta + \int_0^{\infty} dm \int_0^{\infty} d\omega\kappa \times (m^4\kappa^2 + \omega^2)^{-1}\tfrac{1}{2}S(m, \omega), \quad (42c)$$

where $S(m, \omega)$ is the spectrum of vertical shear of both u and v.

4. Estimates of η_e from vertical-shear spectra

In this section we present some straightforward estimates of η_e as given by (7), (36) and (42). Our calculation is based on the empirical vertical-wavenumber spectrum of horizontal shear given by Gargett *et al.* (1981).

a. Description of the shear spectrum

We assume that the shear spectrum is separable (as in most representations of the internal-wave field) with

$$S(\omega, m) = S_1(m)\left(\frac{2f}{\pi}\right)(\omega^2 - f^2)^{-1/2}\omega^{-1}, \quad \text{for} \quad f \leqslant \omega \leqslant N,$$

as in the GM models (e.g., Munk, 1981). For $N/f \gg 1$, as we assume, $\int Nf^{-1}S(m, \omega)d\omega = S_1(m)$. For $S_1(m)$ we adopt the empirical spectrum of Gargett *et al.* (see Fig. 3), i.e.,

$$S_1(m) = \begin{cases} A, & m_0 > m > 0 \\ A(m_0/m), & m_1 > m > m_0 \end{cases} \quad (43)$$

leaving $S_1(m)$ unspecified in the dissipation range $m > m_1$.

b. The transition wavenumber $m_* = (f/\kappa)^{1/2}$

Besides m_0 and m_1, another important landmark in spectral space is the wavenumber at which the transition between the two limits (37a) and (37c) occurs. This wavenumber is

$$m_* = (f/\kappa)^{1/2} = 3 \text{ rad m}^{-1}, \quad \text{if} \quad \kappa = 10^{-5} \text{ m}^{-1} \quad \text{and} \quad f = 10^{-4} \text{ rad s}^{-1},$$

corresponding to

$$\lambda_* = 2\pi/m_* = 2m.$$

Because the shear spectrum $S_1(m)$ monotonically decreases if $m < m_1$, and because of the term m^4 in the denominator of (42), we expect that only wavenumbers $< m_*$ will contribute to horizontal shear dispersion. This expectation is confirmed by the calculation in the next subsection.

c. Calculation of η_e from (42) and (43)

Substitution of (43) into (42c) gives

$$\eta_e = \eta + \kappa \int_f^N d\omega \int_0^\infty dm(\omega^2 + m^4\kappa^2)^{-1} \times (f\pi^{-1})(\omega^2 - f^2)^{-1/2}\omega^{-1}S_1(m).$$

In principle there is no difficulty in doing the integral above exactly using $S_1(m)$ from (43). However it is much simpler to observe that if

$$m > m_* = (f/\kappa)^{1/2}$$

then the integrand is very small. Thus we obtain an adequate estimate of η_e by using the approximation

$$(\omega^2 + m^4\kappa^2)^{-1} \approx \omega^{-2}$$

and the result

$$\frac{f}{\pi}\int_f^N (\omega^2 - f^2)^{-1/2}\omega^{-3}d\omega \approx \tfrac{1}{4}f^{-2},$$

to reduce the expression to

$$\eta_e = \eta + \tfrac{1}{4}\kappa f^{-2}\int_0^{m_*} dmS_1(m),$$
$$= \eta + \tfrac{1}{4}A\kappa f^{-2}m_0[1 + \ln(m_*/m_0)]. \quad (45)$$

Note that the effective horizontal diffusivity depends only on the quasi-universal parameters A and m_0. Taking

$$\left.\begin{aligned} A &\approx 2\times 10^{-4}\ \mathrm{s^{-2}(cpm)^{-1}}, & f &\approx 10^{-4}\ \mathrm{s^{-1}} \\ m_0 &\approx 0.1\ \mathrm{cpm}, & \kappa &\approx 10^{-5}\ \mathrm{m^2\ s^{-1}} \end{aligned}\right\}$$

gives

$$\eta_e - \eta \approx 0.013\ \mathrm{m^2\ s^{-1}} \approx 1300\kappa.$$

Apart from the logarithmic correction in (45), $\eta_e - \eta$ is directly proportional to κ. This shows that horizontal shear dispersion by the internal-wave field is dominated by the Okubo mechanism discussed in Section 2, rather than Taylor's mechanism which would lead to an inverse dependence on κ. The one point to note is that α^2 in (7) is not the total mean-square shear, but rather the mean-square shear in vertical length scales larger than λ_*.

d. Some remarks on η_e in the deep ocean.

The preceding calculation was based on vertical shears observed in the mid-thermocline (recall $N = 4\times 10^{-3}\ \mathrm{s^{-1}} = 40f$). Deeper in the ocean the mean-square shear scales like N^2, and the vertical wavenumber like N, in the sense that

$$S(m, \omega; N) = (N^2/N_0^2)S(\omega, m(N_0/N); N_0).$$

However, Gargett *et al.* (1981) claim there is still a kink at $m_0 = 0.1$ cpm and the Richardson number based on the total shear at wavenumbers $<m_0$ is constant and close to 1. This suggests that in the deep ocean

$$\eta_e - \eta \approx \left(\frac{N}{f}\right)^2\kappa,$$

as claimed by Garrett and Munk (1972) with the same physical process in mind but without the supporting calculations.

e. Significance of steady shear dispersion.

There are other processes of course which produce enhanced horizontal spreading. One that is easily accessible using the arguments developed in this article is steady vertical shear due to mesoscale currents or finestructure in the temperature-salinity fields. It is straightforward to repeat the calculation of Section 2 with a velocity field of the form

$$u = \bar{\alpha}z + \alpha' z\cos\omega t.$$

If $\alpha' \gg \bar{\alpha}$ one finds that the width of a Gaussian stripe initially increases as $t^{1/2}$ because of the oscillatory component but at

$$t \sim \frac{\alpha'}{\bar{\alpha}}\frac{1}{\omega} \sim \left(\frac{\text{inertial shear}}{\text{mean shear}}\right)\left(\frac{\text{inertial period}}{2\pi}\right),$$

the persistent mean shear begins to dominate and produces a $t^{3/2}$ expansion as in Section 5. If we assume that the mean shear is due to mesoscale eddies and take $\bar{\alpha} \sim 10^{-4}\ \mathrm{s^{-1}}$ and $\alpha' \sim 5\times 10^{-3}\ \mathrm{s^{-1}}$, we find $t \sim 6$ days. If significant quasi-steady horizontal velocity exists at the scale of a few meters due to finestructure production, the relevant $\bar{\alpha}$ might be considerably larger than the above estimate, and the steady-shear-dispersion results correspondingly more important.

5. Steady velocity fields: a comparison of shear with strain

In this section we shall discuss diffusion in steady velocity fields. This limit ($\omega \to 0$) is probably more appropriate as a model of horizontal dispersion by the mesoscale eddies. Indeed, a strong motivation for considering the steady limit is to determine the horizontal length scale below which the mesoscale eddies effectively act as steady shears and strains. We also use the results of this section in the conclusion to estimate the horizontal length scale at which the isotropic diffusion due to internal-wave-shear dispersion is as strong as mesoscale shear and strain distortion.

The solution of (1) when $\omega = 0$ can be found by simply taking the limit $\omega \to 0$ in (6). Note how the first term in the Taylor series expansion of $\sin 2\omega t$ cancels and we are left with

$$\theta = \cos k\hat{x}\exp(-\eta k^2 t - \tfrac{1}{3}\kappa\alpha^2k^2t^3), \quad (46)$$

$$\hat{x} = x - \alpha z t. \quad (47)$$

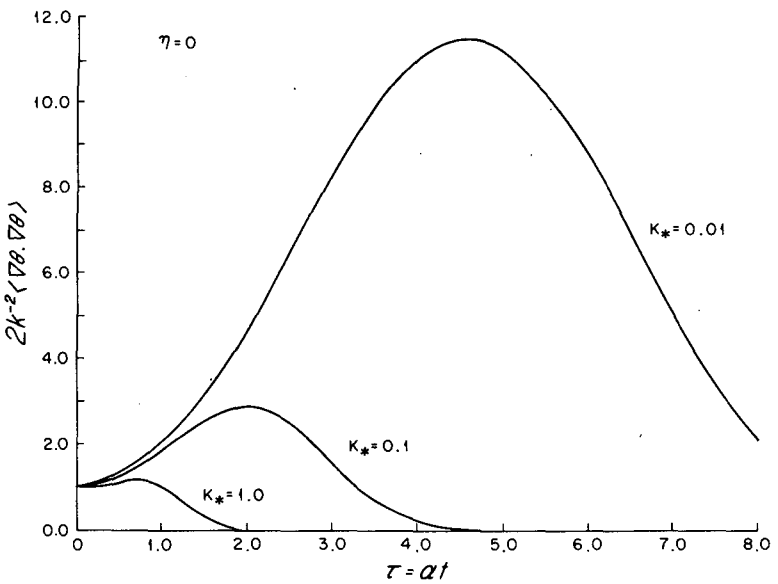

FIG. 4. The growth and eventual decay of the average squared θ gradients in a steady shear flow for different values of the nondimensional diffusivity $\kappa_* = k^2\kappa\alpha^{-1}$.

As $t \to \infty$ the above solution decays much more rapidly than (6), because the steady velocity field, unlike the oscillating field, persistently increases the θ gradients and enhances the diffusion. This point is illustrated more graphically when we consider the evolution of the "Gaussian stripe" initial condition (8). The solution is

$$\theta(x, z, t) = \frac{\pi}{2\tilde{a}} \exp(-\tilde{x}^2/4\tilde{a}^2),$$

where $\tilde{x}$ is given by (47) and

$$\tilde{a}^2 = a^2 + \eta t + \tfrac{1}{3}\kappa\alpha^2 t^3. \qquad (48)$$

The above result is for a "stripe" initial condition, which is the same as the vertical average of a "spot". However, Smith (1982a) has noted that at any given level for a "spot" release the width of the tracer has variance $a^2 + \eta t + (1/12)\kappa\alpha^2 t^3$. As stressed by Okubo (1967) it is impossible to define an effective horizontal diffusivity in this steady-shear-flow problem since it is clear from (48) that the patch expands much more rapidly than can be explained by an ordinary constant Fickian diffusivity. Saffman (1962), using the moment method, found a similar $t^{3/2}$ growth in the width of a cloud released at ground level into a semi-infinite atmosphere in which the velocity increases linearly with z.

Coincidentally the $t^{3/2}$ expansion of the length scale in (48) is identical to that predicted by Richardson's "neighbour separation" theory of relative diffusion in a turbulent flow. In this turbulence problem the faster-than-$t^{1/2}$ spreading occurs because a larger range of eddy sizes can act on the patch as its scale increases. This mechanism is very different from that in (48) where the $t^{3/2}$ behavior is produced by vertical diffusion from faster flowing regions into slowly flowing levels. The point is that one should not be too hasty in attributing $t^{3/2}$ patch growth to relative diffusion, for a steady shear flow is capable of producing the same behavior.

a. Wavenumber cascade and enhanced diffusion in a steady shear

To quantify the notion that the shear flow amplifies the θ gradients until the enhanced diffusion rapidly destroys them it is informative to compute the x-average average of $\nabla\theta \cdot \nabla\theta$:

$$\langle \nabla\theta \cdot \nabla\theta \rangle = \lim_{L\to\infty} \frac{1}{2L} \int_{-L}^{L} \nabla\theta \cdot \nabla\theta dx$$

$$= \tfrac{1}{2}k^2[1 + (\alpha t)^2] \exp(-2\eta k^2 t - \tfrac{2}{3}\kappa\alpha^2 k^2 t^3). \qquad (49)$$

The right-hand side of (49) is plotted as a function of the nondimensional time $\tau = (\alpha t)$ in Fig. 4. The initial growth and eventual decay of the θ gradients is as expected. This figure is a vivid example of the distinction made between mixing and stirring by Eckart (1948). The initial growth in the mean-square gradients is due to stirring while the rapid decay is due to molecular mixing enhanced by advection. What is not so obvious physically is what determines the time $\tau_* = \alpha t_*$ at which the averaged squared gradient is a maximum. From (49) it easily follows that

$$\tau_* - (\eta_* + \kappa_* \tau_*^2)(1 + \tau_*^2) = 0, \qquad (50)$$

where

$$\eta_* = \eta k^2/\alpha \quad \text{and} \quad \kappa_* = \kappa k^2/\alpha$$

are nondimensional diffusivities (not to be confused with the κ_* defined in Section 3). If $\eta_* = O(\kappa_*)$ and $\kappa_* \ll 1$, the relevant solution of the quartic is

$$\tau_* = \kappa_*^{-1/3} - \tfrac{1}{3}\kappa_*\left(1 + \frac{\eta_*}{\kappa_*}\right) + O(\kappa_*^{7/3}).$$

Reverting to dimensional units the above is

$$\alpha t_* = \left(\frac{\alpha}{\kappa k^2}\right)^{1/3} + \text{smaller terms.} \qquad (51)$$

The ⅓-power in (51) can be explained physically by forming the equation for the time rate of change of $\langle \nabla\theta \cdot \nabla\theta \rangle$. From (1) one has

$$\langle \tfrac{1}{2}\nabla\theta \cdot \nabla\theta \rangle_t + \alpha\langle \theta_x\theta_z \rangle = -\eta \langle \nabla\theta_x \cdot \nabla\theta_x \rangle - \kappa\langle \nabla\theta_z \cdot \nabla\theta_z \rangle, \qquad (52)$$

where the angle brackets denote a spatial average. The first term in (52) increases initially because the shear creates some θ_z and so the second term grows. Eventually, however, the third and fourth terms dominate and the first term decreases. The maximum value of $\langle \nabla\theta \cdot \nabla\theta \rangle$ is then achieved when the second and fourth terms have equal magnitudes. The time at which this occurs can be estimated using the following relations which apply at $t \to \infty$:

$$\frac{\partial}{\partial x} \sim k \quad \frac{\partial}{\partial z} \sim \nabla \sim k\alpha t.$$

It follows that

$$\alpha\langle \theta_x\theta_z \rangle \sim \alpha k^2(\alpha t),$$
$$\kappa\langle \nabla\theta_z \cdot \nabla\theta_z \rangle \sim (\alpha t)^4 \kappa k^4,$$

when the right-hand sides of the above are equated, (51) is recovered. Note that if one naively estimated t_* as the time at which the shear time scale α^{-1} equaled the diffusion time scale based on the decreasing length scale of the tracer distribution, $[\kappa(k\alpha t)^2]^{-1}$, the answer, $\alpha t_* = (\alpha/\kappa k^2)^{1/2}$, would be wrong; see (51).

It is interesting to calculate t_* from (51) for numbers typical of the mesoscale eddy field. As a typical shear, suppose the velocity changes by 10 cm s^{-1} in 100 km; then

$$\alpha \sim 10^{-6}\ s^{-1}.$$

For κ, suppose that the mesoscale eddies "feel" an effective horizontal diffusivity due to shear dispersion by internal waves. The calculation in Section 4 gives

$$\kappa = \eta_e \sim 0.01\ m^2\ s^{-1};$$

hence for a 100 km wide patch of tracer

$$k = \frac{2\pi}{10^5\ m} \quad \text{implies} \quad \alpha t_* \sim 13.5$$
$$\text{or} \quad t_* \sim 5\tfrac{1}{2} \text{ months},$$

while for a 5 km patch

$$k = \frac{2\pi}{5 \times 10^3\ m} \quad \text{implies} \quad \alpha t_* \sim 4$$
$$\text{or} \quad t_* \sim 1\tfrac{1}{2} \text{ months}.$$

Thus, the temporal variability of the mesoscale eddies is significant for tracer anomalies with horizontal length scales of 100 km since it takes a steady shear field ~6 months to amplify the gradients to the point where diffusivity arrests the wavenumber cascade. On the other hand, tracer anomalies with length scales ≤5 km are so small that their mean-square gradients peak and decay before the mesoscale field changes significantly.

These estimates are based on the effects of a steady shear "orthogonal" to the tracer; they will have to be revised in the light of a steady strain model discussed in the next subsection and also in situations where the tracer has become uniform along streamlines (as in a well mixed eddy).

b. *Wavenumber cascade and enhanced diffusion in a steady strain*

This completes our discussion of diffusion in a steady *shear*. To conclude this section we will contrast this solution with one previously discussed by Townsend (1951), Batchelor (1959) and Phillips (1977) for diffusion in a steady *strain*. There are important qualitative differences between the two. Consider the pure straining field

$$(u, w) = (\beta x, -\beta z) \quad \text{and} \quad \beta > 0.$$

The passive tracer θ satisfies

$$\theta_t + \beta x\theta_x - \beta z\theta_z = \eta\nabla^2\theta, \qquad (53)$$

where for simplicity we have assumed an isotropic diffusivity. To solve (53) we begin by setting $\eta = 0$. The solution of the resulting advection equation which satisfies the initial condition (2) is

$$\theta(x, z, t) = \cos(ke^{-\beta t}x)\cos(me^{\beta t}z). \qquad (54)$$

Note how the strain increases the z wavenumber exponentially with time; the shear only produced a growth linear in time. In such a strain field the particle paths, $(x, z) = (x_0e^{-\beta t}, z_0e^{\beta t})$, imply a one-particle diffusivity

$$\frac{1}{2}\frac{d}{dt}[(x - x_0)^2 + (z - z_0)^2] \sim \beta z_0^2 e^{2\beta t},$$

if $\beta t \gg 1$. The two-particle diffusivity, which is

$$\frac{1}{2}\frac{d}{dt}[(x_2 - x_1)^2 + (z_2 - z_1)^2],$$

corresponding to particles 1 and 2, is also proportional to $e^{2\beta t}$ if $\beta t \gg 1$. Similar exponential particle separation is found in the inertial range of two-dimensional turbulence. Thus, exponentially growing two-particle separations are not necessarily due to turbulent eddies of many sizes.

To solve (55) with $\eta \neq 0$ we look for a solution of the form

$$\theta(x, z, t) = A(t)\cos(ke^{-\beta t}x)\cos(me^{\beta t}z). \quad (55)$$

When (55) is substituted into (53) and the resulting equation for A is solved there results

$$\theta(x, z, t) = \exp\left\{\frac{\eta}{2\beta}[k^2(e^{-2\beta t} - 1) - m^2(e^{2\beta t} - 1)]\right\}$$

$$\times \cos(ke^{-\beta t}x)\cos(me^{\beta t}z) \to \exp\left\{-\left(\frac{\eta m^2}{2\beta}\right)e^{2\beta t}\right\}$$

$$\times \cos(ke^{-\beta t}x)\cos(me^{\beta t}z) \quad \text{as} \quad t \to \infty. \quad (56)$$

Comparing (56) with (46) it is clear that straining fields are much more effective than shearing fields at producing transfers to high wavenumbers and enhancing diffusion. One method of quantifying this is to calculate $\langle \nabla\theta \cdot \nabla\theta \rangle$ from (56); for simplicity we suppose $m = k$, in which case

$$\langle \nabla\theta \cdot \nabla\theta \rangle = \tfrac{1}{2}k^2 \cosh(2\beta t) \times \exp\left[-\left(\frac{2\eta k^2}{\beta}\right)\sinh 2\beta t\right]. \quad (57)$$

This exhibits the same qualitative behavior as (49), an initial increase to a maximum followed by a rapid decrease to zero. The time at which the gradients are largest when $\eta k^2/\beta \ll 1$ is

$$2\beta t_* = \ln[\beta/\eta k^2] + (\text{smaller terms}), \quad (58)$$

which should be compared to (51). In contrast to the shear problem t_* in (58) is equal to the time at which the time scale β^{-1} of the strain equals the diffusion time based on the length scale of the tracer, $[\kappa k^2 e^{2\beta t}]^{-1}$. If α^{-1} and β^{-1} are comparable time scales we see that $\langle \nabla\theta \cdot \nabla\theta \rangle$ peaks at a smaller time in a straining field. To emphasize this point we will again estimate t_* using values of β and η typical of the mesoscale eddies. Taking $\beta \sim 10^{-6}$ s^{-1}, $\eta = 0.01$ m^2 s^{-1} and $k = 2\pi/10^5$ m, one has from (58)

$$t_* \approx 4 \times 10^6 \text{ s} \approx 2 \text{ months},$$

while for $k = 2\pi/5 \times 10^3$ m

$$t_* \approx 2 \times 10^6 \text{ s} \approx 3 \text{ weeks}.$$

Thus at length scales of 100 km the difference in t_* between a shearing and straining field is significant, although in both cases t_* is so long that temporal variability is probably important. The reduction in t_* at length scales of 5 km is less marked although still present. Our earlier conclusion that anomalies on these small length scales cascade through wavenumber space and then suffer accelerated diffusive decay in a "frozen" mesoscale field is reinforced. One should note, however, that this calculation may overestimate the efficacy of "strain" dispersion since its hyper-exponential time behavior relies in part on the large velocities as $|x|$ and $|z| \to \infty$. It would be informative to investigate a model containing both shear and strain (e.g., $\psi \propto \sin x \sin z$) numerically.

6. Conclusion

In this article we have been primarily concerned with parameterizing the horizontal mixing due to the interaction of vertical mixing with the vertical shear of inertial oscillations [see (42)]. The simple exact solutions and geometric argument of Section 2 are intended to make this weighted integral of the vertical-shear spectrum comprehensible in physical terms. The most optimistic interpretation of our results is that the effective horizontal diffusivity so calculated is that which is "felt" by the turbulent mesoscale eddy field. This naive notion was used in Section 4 to argue that the temporal variability of the mesoscale becomes important for tracer anomalies with length scales $\gtrsim$5 km. Below this scale tracer anomalies cascade through wavenumber space and suffer enhanced diffusion in a "frozen" mesoscale field.

To conclude we will estimate the horizontal length scale at which the horizontal stirring due to turbulent geostrophic eddies balances horizontal diffusion due to inertial oscillations. To see what is meant by this imagine releasing a very small blob of passive tracer. Initially the blob expands due to the shear dispersion mechanism,

$$\frac{d\overline{a^2}}{dt} = 2\eta_e, \quad (59)$$

where $\overline{a^2}$ is the mean square width of the patch. When the patch reaches a certain transition scale, however, the mean-square width increases exponentially due to the turbulent mesoscale

$$\frac{d\overline{a^2}}{dt} = \mu\overline{a^2}, \quad (60)$$

where μ is related to the rms strain rate of the mesoscale. [For a review of the arguments leading to (60), see Kraichnan and Montgomery (1980).] Float data (based on separations >30 km) analyzed by Price (1981) suggest μ is somewhere between 2×10^{-7} s^{-1} and 10^{-6} s^{-1} in the western Sargasso Sea.

If we assume the vertical diffusivity is 10^{-5} m^2 s^{-1} then the calculation in Section 4 based on the empirical vertical shear spectrum gives $\eta_e = 10^{-2}$ m^2 s^{-1}. The transition scale between (59) and (60) is estimated by equating the right-hand sides. One finds $(\overline{a^2})^{1/2}$ is between 100 and 500 m. Thus mesoscale stirring begins to dominate at surprisingly small length scales. This small transition scale does not imply that inertial shear dispersion is unimportant since we hypothesize that it is the endpoint of the cascade of tracer variance through wavenumber space. The physical-space equivalent of this cascade is a well-known tendency of two-dimensional velocity fields to "tease" passive scalar fields (and vorticity) out into filaments. This process is arrested by η_e which prevents the straining velocity from compressing the width of the filaments below the transition scale $(\mu/\eta_e)^{1/2} \sim (\eta_e/\mu)^{1/2} \sim$ 100–500 m.

Acknowledgments. P.B.R. and W.R.Y. are supported by National Science Foundation Grant OCE 78-25692. C.J.R.G. is supported by the Natural Sciences and Engineering Research Council of Canada, and by the Guggenheim Foundation.

W.R.Y. wishes to thank R. Schmitt and R. Smith for several enlightening conversations during the course of this work.

REFERENCES

Aris, R., 1956: On the dispersion of a solute in a fluid flowing through a tube. *Proc. Roy. Soc. London*, **A235,** 67–77.

Batchelor, G. K., 1959: Small scale variation of convected quantities like temperature in a turbulent field. Part I. General discussion and the case of small conductivity. *J. Fluid Mech.*, **5,** 113–133.

Bowden, K. F., 1965: Horizontal mixing in the sea due to a shearing current. *J. Fluid Mech.*, **21,** 83–95.

Chatwin, P. C., 1975: On the longitudinal dispersion of passive contaminant in oscillatory flows in tubes. *J. Fluid Mech.*, **71,** 513–527.

Csanady, G. T., 1966: Diffusion in an Ekman layer. *J. Atmos. Sci.*, **26,** 414–426.

Eckart, C., 1948: An analysis of the stirring and mixing processes in incompressible fluids. *J. Mar. Res.*, **7,** 265–275.

Fischer, H. B., 1976: Mixing and dispersion in estuaries. *Annual Review of Fluid Mechanics*, Vol. 8, Annual Reviews, Inc., 107–133.

——, E. J. List, R. C. Y. Koh, J. Imberger and N. H. Brooks, 1979: *Mixing in Inland and Coastal Waters*. Academic Press, 483 pp.

Gargett, A. E., P. J. Hendricks, T. B. Sanford, T. R. Osborn and A. J. Williams, III, 1981: A composite spectrum of vertical shear in the upper ocean. *J. Phys. Oceanogr.*, **11,** 1258–1271.

Garrett, C. J. R., and W. H. Munk, 1972: Oceanic mixing by breaking internal waves. *Deep-Sea Res.*, **19,** 823–832.

——, and J. W. Loder, 1981: Dynamical aspects of shallow sea fronts. *Circulation and Fronts in Continental Shelf Seas*, J. C. Swallow, R. I. Currie, A. E. Gill and J. H. Simpson, Eds., Royal Society of London, 563–581.

Kraichnan, R. H., and D. Montgomery, 1980: Two-dimensional turbulence. *Rep. Prog. Phys.*, **43,** 547–619.

Kullenberg, G., 1972: Apparent horizontal diffusion in a stratified vertical shear flow. *Tellus*, **24,** 17–28.

Munk, W. H., 1981: Internal waves and small scale processes. *Evolution of Physical Oceanography*, B. A. Warren and C. Wunsch, Eds., MIT Press, 264–291.

Okubo, A., 1967: The effect of shear in an oscillatory current on horizontal diffusion from an instantaneous source. *Int. J. Oceanogr. Limnol.*, **1,** 194–204.

Phillips, O. M., 1977: *The Dynamics of the Upper Ocean*, 2nd ed. Cambridge University Press, 336 pp.

Price, J., 1981: Diffusion statistics computed from SOFAR float trajectories in the western North Atlantic (Unpublished Proceedings CAMS-WHOI Symposium on Lagrangian Tracers, Woods Hole.

Saffman, P. G., 1962: The effect of wind shear on horizontal spread from an instantaneous ground source. *Quart. J. Roy. Meteor. Soc.*, **88,** 382–393.

Smith, R., 1982a: The memory paradox for contaminant dispersion in the deep ocean. Submitted to *J. Fluid Mech.*

——, 1982b: Contaminant dispersion in oscillatory flows. *J. Fluid Mech.*, **114,** 379–398.

Taylor, G. I., 1953: Dispersion of soluble matter in solvent flowing slowly through a tube. *Proc. Roy. Soc. London*, **A219,** 186–203.

Townsend, A. A., 1951: The diffusion of heat spots in isotropic turbulence. *Proc. Roy. Soc. London*, **A209,** 418–430.